Journal of Medicinal Chemistry

ARTICLE

pubs.acs.org/jmc

Novel Hydrazine Molecules as Tools To Understand the Flexibility of Vascular Adhesion Protein-1 Ligand-Binding Site: Toward More Selective Inhibitors

Elisa M. Nurminen,[†] Marjo Pihlavisto,[‡] László Lázár,[§] Ulla Pentikäinen,[†] Ferenc Fülöp,[§] and Olli T. Pentikäinen*[,†]

[†]Department of Biological and Environmental Science and Nanoscience Center, University of Jyväskylä, P.O. Box 35, FI-40014 Jyväskylä, Finland

[‡]BioTie Therapies Corporation, Tykistökatu 6, FI-20520 Turku, Finland

[§]Institute of Pharmaceutical Chemistry, University of Szeged, H-6720 Eotvos 6, Szeged, Hungary

ABSTRACT: Vascular adhesion protein-1 (VAP-1) belongs to a family of amine oxidases. It plays a role in leukocyte trafficking and in amine compound metabolism. VAP-1 is linked to various diseases, such as Alzheimer's disease, psoriasis, depression, diabetes, and obesity. Accordingly, selective inhibitors of VAP-1 could potentially be used to treat those diseases. In this study, eight novel VAP-1 hydrazine derivatives were synthesized and their VAP-1 and monoamine oxidase (MAO) inhibition ability was determined in vitro. MD simulations of VAP-1 with these new molecules reveal that the VAP-1 ligand-binding pocket is flexible and capable of fitting substantially larger ligands than was previously believed. The increase in the size of the VAP-1 ligands, together with the methylation of the secondary nitrogen atom of the hydrazine moiety, improves the VAP-1 selectivity over MAO.

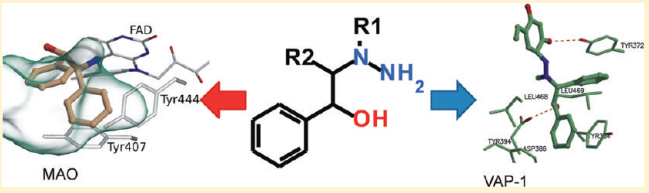

Amine oxidases (AOs) are enzymes that metabolize diverse amine compounds by converting them into corresponding aldehydes with concomitant hydrogen peroxide and ammonia production. AOs can be divided into two families based on their cofactors. The first family of AOs includes monoamine oxidases A and B (MAOs A and B, EC 1.4.3.4.) and polyamine oxidase (EC 1.5.3.11.), which have flavin adenosine dinucleotide as a cofactor. The second family of AOs include diamine oxidase (DAO, EC 1.4.3.22.), lysyl oxidase (EC 1.4.3.13.), and vascular adhesion protein-1 (VAP-1, EC 1.4.3.21.), which all have modified tyrosine (topaquinone, TPQ) or lysine residue as a cofactor.

VAP-1 is an interesting member of the AO family. In addition to being an enzyme, it also has an adhesive task in leukocyte extravasation.[1] VAP-1 is a type II transmembrane glycoprotein with a large glycosylated extracellular domain and a short N-terminal intracellular domain, which is involved in the adhesion of lymphocytes to endothelial cells and lymphocyte recirculation.[1] VAP-1 is primarily expressed on endothelial cells, but some expression is also detected in nonendothelial cells, e.g., blood vessel smooth muscle cells.[2] VAP-1 activity can exert insulin-like effects on glucose metabolism via hydrogen peroxide.[3] Hydrogen peroxide acts as a local signaling molecule, but excess amounts can cause oxidative stress. Other reaction products are potential toxins as well; for example, methylglyoxal can form advanced glycation end products.[4] Maintenance of constant levels of the reaction products is crucial because in normal concentrations, they are beneficial and necessary, but increased or decreased amounts can cause severe diseases. Alterations in reaction product levels and corresponding diseases can arise from either overexpression[5−11] or underexpression of VAP-1[12−16] or from increased enzymatic activities of VAP-1.[17−22]

VAP-1 is a potential target for drug development because it is involved in many diseases. Various VAP-1 inhibitors have already been developed, such as phenylallylhydrazines[23] thiocarbamoyl derivatives,[24] carboxamides and sulfonamides,[25] and hydrazines[1,26] (Figure 1). VAP-1 function can also be modulated by using (1) peptides with NH_3^+ functionality (lysine side chain),[27−29] (2) function blocking antibodies (to inhibit the leukocyte trafficking),[30] and (3) small interfering RNAs (to inhibit both adhesion and enzymatic functions).[31] Because amine oxidases have partly overlapping substrate specificities, it is challenging to design selective inhibitors for one member of an AO family. The compounds mentioned above establish a promising starting point for VAP-1 blocking pharmaceuticals, but they are not selective or safe enough yet.

The crystal structures determined for human VAP-1[32−34] show that the structure of VAP-1 is homodimeric. The active site is located near the dimerization interface, buried deep within the protein, and includes the TPQ cofactor and the catalytic base (Asp386).[32−34] The accessibility of the active site is restricted by Leu469, which blocks the entrance to the ligand-binding site.[34]

We have recently reported that hydrazine derivatives are potential selective VAP-1 inhibitors.[26] The reaction mechanism

Received: October 17, 2010
Published: March 15, 2011

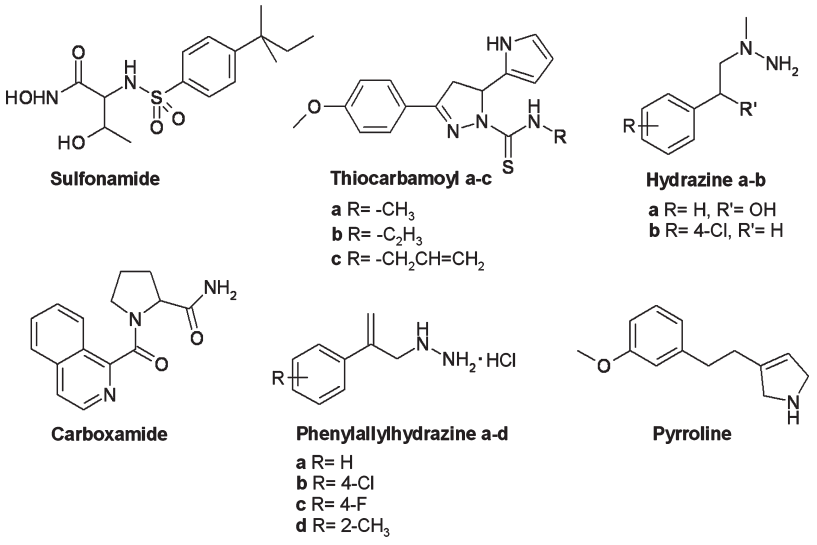

Figure 1. Structures of some known small molecule VAP-1 inhibitors: phenylallylhydrazines,[23] thiocarbamoyl derivatives,[24] carboxamides and sulfonamides,[25] hydrazines,[1,26] and pyrroline derivatives.[63]

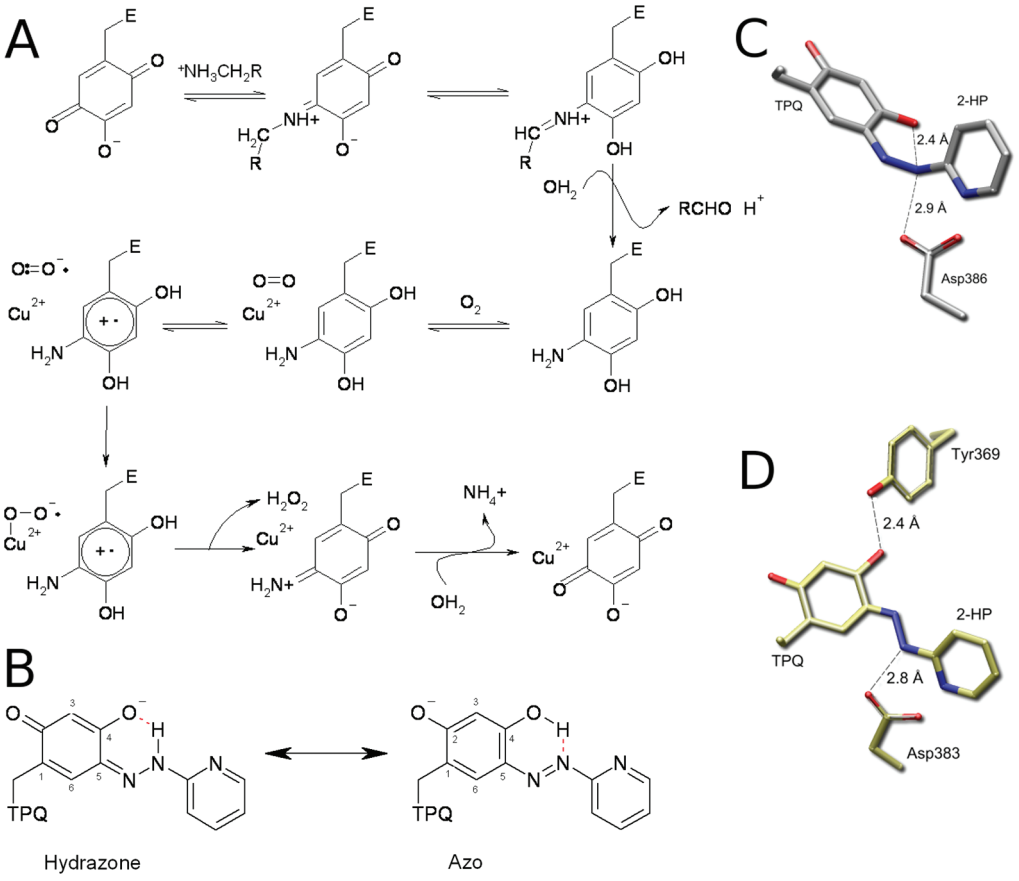

Figure 2. Binding of 2-hydrazinopyridine (2-HP) to TPQ: (A) reaction mechanism of VAP-1;[36] (B) resonance structures of 2-HP−TPQ complex, the prevalent hydrazone form in physiological pH and the distinctive azo form, detected at pH > 9; (C) 3D crystal structure of bound 2-HP in human VAP-1 (PDB code 2C11[33]); (D) 3D crystal structure of 2-HP in *E. coli* amine oxidase (PDB code 1SPU[35]).

of the TPQ catalyzed reaction has been studied extensively (Figure 2A), and it appears that the efficacy of hydrazine molecules to inhibit copper amine oxidases is based on their ability to form a mimic of the substrate Schiff base intermediate with the enzyme.[35] In the case of a natural substrate, the catalytic aspartic acid participates in the deamination reaction where its role is to abstract a proton from the natural substrate. When a hydrazine compound is bound, instead of a substrate molecule,

dx.doi.org/10.1021/jm200059p |*J. Med. Chem.* 2011, 54, 2143–2154

Table 1. Novel VAP-1 Inhibitor Compounds

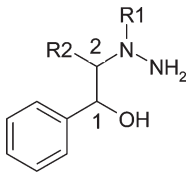

compd	R1	R2	relative configuration	IC_{50} VAP-1 (μM)[a]	IC_{50} MAO (μM)[b]	selectivity[c]
2a	H	H	1*R*	0.04 ± 0.01	9.90 ± 2.20	250
2b	H	H	1*S*	0.15 ± 0.01	9.80 ± 1.00	65
5	H	C_6H_5	1*R**,2*S**	50 ± 3	34 ± 3	0.7
8	H	$(CH_2)_2CH_3$	*d*	1.20 ± 0.16	11 ± 2	9
11a	CH_3	C_6H_5	1*R*,2*S*	0.28 ± 0.03	70 ± 12	250
11b	CH_3	C_6H_5	1*S*,2*S*	1.18 ± 0.08	85 ± 9	72
11c	CH_3	C_6H_5	1*R*,2*R*	1.06 ± 0.04	99 ± 10	90
11d	CH_3	C_6H_5	1*S*,2*R*	0.33 ± 0.02	105 ± 13	320
12[e]	CH_3	$(CH_2)_2CH_3$	1*R**,2*S**	0.26 ± 0.04	28 ± 1	110

[a] IC_{50} data for VAP-1 in μM, mean ± SEM of two to four similar experiments. [b] IC_{50} data for MAO in μM, mean ± SEM of two to four similar experiments. [c] Calculated IC_{50}(MAO)/IC_{50}(VAP-1). [d] Mixture of diastereomers. [e] Reference 26.

the enzymatic reaction is halted because the catalytic aspartic acid cannot abstract a proton from the secondary amine group.[35] The reactivity of the hydrazines also makes these molecules excellent inhibitors for AOs.

The available 3D crystal structure of VAP-1 with bound inhibitor 2-hydrazinopyridine (PDB code 2C11[33]) shows the general mechanism by which an unsubstituted hydrazine binds to VAP-1 (Figure 2B and Figure 2C). The primary amine group of the hydrazine binds covalently to the TPQ cofactor. The secondary amine group of the hydrazine participates in a hydrogen bond, with the C4 oxygen of the TPQ (Figure 2B and Figure 2C), with the Asp386 carboxyl group, or with both (Figure 2D). This strongly determines the conformation of the rest of a molecule.[36] On the basis of the crystal structure of VAP-1 with 2-hydrazinopyridine (PDB code 2C11[33]), the distances and angles from the secondary nitrogen atom to the C4 oxygen atom of the TPQ cofactor and the Asp386 carboxylate group are appropriate for hydrogen bonding, suggesting a positively charged amine group (Figure 2C). The crystal structure of *Escherichia coli* amine oxidase, in complex with 2-hydrazinopyridine (1SPU[35]), demonstrates another type of binding. In this complex structure, the C4 oxygen atom of the TPQ is situated close to the conserved Tyr369, which suggests a shared proton[35] (Figure 2D). The secondary amine of the 2-hydrazinopyridine turns toward the C6 of the TPQ rather than toward C4, as it does in the 2C11 structure,[33] showing that hydrogen bonding of the secondary amine group occurs to catalytic Asp383 and in the main chain of Val463. Furthermore, this also suggests a positively charged secondary amine group.

The previously published three-dimensional quantitative structure−activity relationship model of VAP-1 hydrazine-derived inhibitors[26] predicted that the larger ligands could show even higher VAP-1 selectivity over MAO than was earlier reported. Here, we have designed, synthesized, and tested the in vitro VAP-1 and MAO inhibition potency of eight novel hydrazine molecules that substantially enlarge the understanding of VAP-1 flexibility and its inhibitor binding capability. These molecules show high VAP-1 selectivity over MAO. Additionally, molecular dynamics (MD) simulations were used to study the effect of bulky inhibitor binding onto the VAP-1 structure. These simulations visualize the high reorganization capability of the amino acids that line the ligand-binding cavity, providing a new, extra space to accommodate the ligands. This space could be utilized in the development of new, better, and more selective VAP-1 inhibitors. We also show that, compared to the 2-hydrazinopyridine and other nonsubstituted hydrazine molecules, substitution on the secondary amine group results in a distinct binding mode.

RESULTS AND DISCUSSION

Design of Novel Hydrazines. Previously, we reported the construction of 3D-QSAR models, based on 47 hydrazine molecules and their IC_{50} values for VAP-1 and MAO.[26] The VAP-1 model suggested that introduction of steric groups to position C2 (Table 1) would be beneficial for VAP-1 potency. Therefore, we designed a small series of novel hydrazine molecules with varied C2 substituents. The molecules used for model building were smaller than the newly designed molecules (Table 1). Thus, the prediction of novel molecules, using the QSAR model, was omitted prior to the synthesis and the in vitro testing of molecules.

Synthesis. In the syntheses of **2a**,**b**, **5**, **8**, and **11a**−**d**, conventional methods for the preparation of hydrazino alcohols[37] were applied. Enantiomers of 2-hydrazino-1-phenylethanol (**2a**,**b**) were prepared by hydrazinolysis of the corresponding (*S*)- or (*R*)-styrene oxide (**1a**,**b**), resulting in a mixture of the regioisomeric products, **2** and **3**, in a ratio of about 2:1, from which the main components (**2a**,**b**) were isolated by fractional crystallization of the hydrogen maleate salt. Similarly, (1*R**,2*S**)-2-hydrazino-1,2-diphenylethanol (**5**) was obtained

Scheme 1[a]

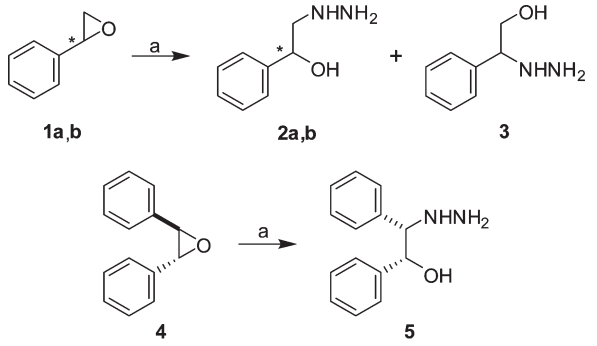

1,**2**: (1*R*): **a**, (1*S*): **b**

[a] Reagents: (a) H_2NNH_2, H_2O, and EtOH (yield, 52−62%).

Scheme 2[a]

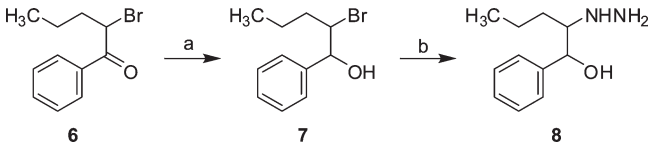

[a] Reagents: (a) $NaBH_4$, MeOH (yield, ∼100%); (b) H_2NNH_2, H_2O, and EtOH (yield, 53%).

from the ring-opening reaction of (±)-*trans*-stilbene oxide (**4**) with hydrazine hydrate (Scheme 1).[38]

A nucleophilic substitution reaction of the corresponding bromo-substituted alcohol (**7**) with hydrazine was applied for the synthesis of 2-hydrazino-1-phenylpentanol (**8**) (Scheme 2).[37,39] Compound **7** was formed as a diastereomeric mixture in the reduction of (±)-2-bromo-1-phenylpentanone[40] (**6**) with $NaBH_4$.[41] All our efforts to separate the diastereomers of **8** have failed.

Isomeric 2-(1-methylhydrazino)-1,2-diphenylethanols **11a**−**d** were prepared from enantiomerically pure amino alcohols **9a**−**d**,[42−44] using a two-step procedure that included N-nitrosation and subsequent $LiAlH_4$ reductions of the *N*-nitroso intermediates **10a**−**d** (Scheme 3).

In Vitro Potency. In vitro potencies were determined for the synthesized inhibitors **2a**,**b**, **5**, **8**, and **11a**−**d** (Table 1). The in vitro potency of **12** was reported earlier.[26] The results indicate that the compounds **2a**, **11a**, and **11d** are highly specific inhibitors of human VAP-1 activity. The IC_{50} for VAP-1 inhibition varies from 50 to 0.04 μM (Table 1). Major differences were found in the selectivity of the inhibitors against the total MAO potency, with selectivity ranging from nonselective to 320-fold selective (Table 1).

Binding of 1*R*- and 1*S*-2-Hydrazinyl-1-phenylethanol to VAP-1. In the crystal structure of VAP-1 with a bound inhibitor, 2-hydrazinopyridine, Leu469 blocks the ligand-binding cavity.[33] However, as we recently reported, during the MD simulations of VAP-1 with inhibitors larger than 2-hydrazinopyridine, Leu469 rotates and unblocks the ligand-binding cavity, providing to the ligands free access from the solvent to the ligand-binding pocket.[26] This rotated Leu469 conformation was used here as the starting structure.

Two stereoisomers of 2-hydrazinyl-1-phenylethanol (1*R* = **2a** and 1*S* = **2b**; Table 1) are the simplest molecules studied in this research. Both stereoisomers were docked to the VAP-1 structural

Scheme 3[a]

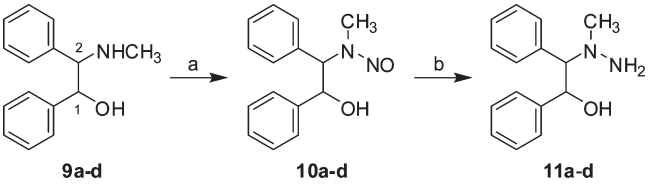

9-**11**: (1*R*,2*S*): **a**, (1*S*,2*S*): **b**, (1*R*,2*R*): **c**, (1*S*,2*R*): **d**

[a] Reagents: (a) $NaNO_2$, AcOH, H_2O (yield, 95−97%); (b) $LiAlH_4$, THF (yield, 58−65%).

model, where Leu469 is rotated, as described above, resulting in a similar binding conformation, as seen in the VAP-1-bound 2-hydrazinopyridine (Figure 2C). To understand the binding of **2a** and **2b** in more detail, MD simulations were used to study the complexes obtained from the docking. These simulations of VAP-1, with bound **2a**,**b**, show that the surrounding amino acids Tyr384, Phe389, Tyr394, Leu468, and Leu469 form a hydrophobic pocket that nicely accommodates the phenyl rings of **2a** and **2b** (Figure 3). Both **2a** and **2b** can form a tight hydrogen bond network (Figure 3), which explains their excellent potency for VAP-1. The orientation of the hydroxyl group (1*R* = **2a** and 1*S* = **2b**) represents the greatest difference in the ability of **2a** and **2b** to bind to VAP-1. The hydroxyl group of **2a** points away from Tyr384, where it has more space (Figure 3A), while the hydroxyl group of **2b** has difficulties accommodating itself between the aromatic rings of Tyr384 and Phe389 (Figure 3B). This may explain why **2a** binds 4 times better to VAP-1 than does **2b**. The binding of **2a** and **2b** induce conformational changes in two amino acid side chains: Met211 and Leu469 (shown with **2a** in Figure 3A). This reveals new free space near C2 of **2a**,**b** (Figure 3).

Effect of Propyl Substitution at C2. Docking simulations indicated that the addition of a propyl group to C2, compound **8** (Table 1), can utilize the additional space (Figure 4A), revealed by the rotation of Met211 and Leu469, during the MD simulation of VAP-1 with bound **2a** and **2b** (parts A and B of Figure 3, respectively). On the basis of the binding of **2a** and **2b** (parts A and B of Figure 3), the 1*R*,2*S* enantiomer of **8** is optimal for binding to VAP-1 because (a) the hydroxyl group can freely interact with the Asp386 and (b) the 2*S*-propyl can accommodate itself into the space formed by the rotation of Met211 and Leu469, during the MD simulation of VAP-1 with bound **2a**,**b** (Figure 4A). Although compound **8** seems to fit into the VAP-1 ligand-binding site, its inhibitory activity is clearly worse than the inhibitory activity of **2a** and **2b** (Table 1).

As previously reported, the methylation of the secondary amine at the hydrazine moiety (N-methylation) can lower the potency of ligands.[26] However, the N-methylation of **8** increases the potency because the IC_{50} value of N-methylated **12** is 0.26 μM while the IC_{50} value of nonmethylated **8** is 1.20 μM (Table 1). In order to study the binding of the N-methylated compound **12** (1*R*,2*S*), it was docked into the VAP-1 conformation obtained from the MD simulations with **2a**. As expected, the N-methylated compound **12** yielded a distinct conformation than did the nonmethylated compound **8** (Figure 4). The *N*-methyl group of **12** points toward the main chain of Leu469, whereas in compound **8**, the hydrogen of the same nitrogen atom is hydrogen-bonded with Asp386 and the hydroxyl group of TPQ (Figure 4). The conformation of **8** is further stabilized by

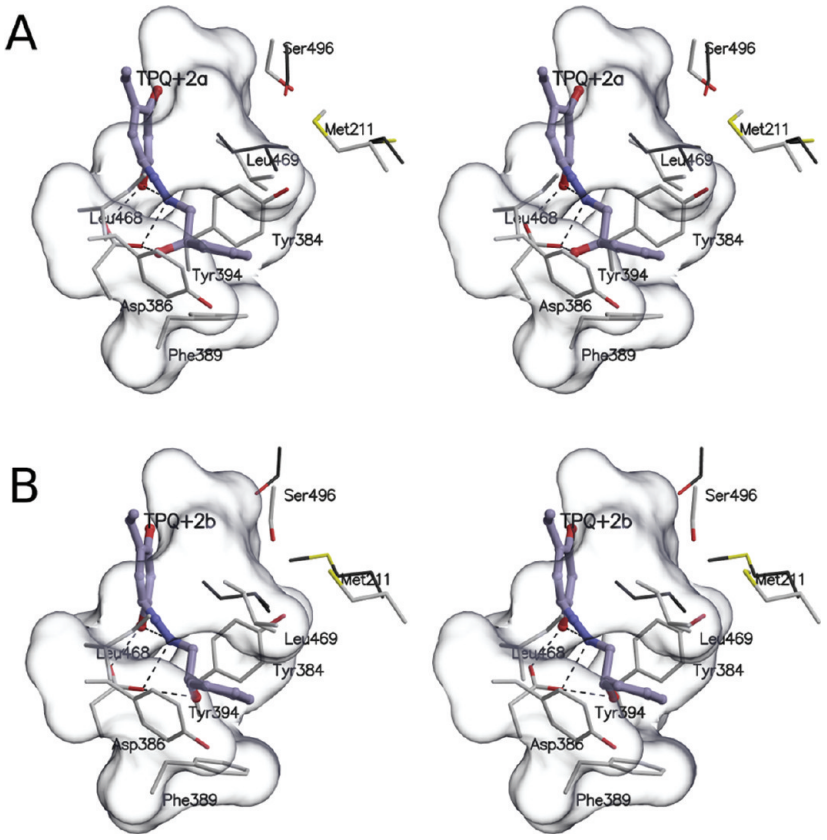

Figure 3. Binding of **2a**,**b** to VAP-1 (parallel stereoview). (A) In the course of MD simulation the side chains of Met211 and Leu469 change their conformation (black sticks) but the rest of the side chains remain close to the starting conformations (gray sticks). TPQ—**2a** is shown in ball-and-stick. The phenyl ring of **2a** is surrounded by hydrophobic Leu468 and Leu469 and aromatic Tyr384, Phe389, and Tyr394 (surface rendering). Multiple hydrogen bonds are present: Asp386 forms hydrogen bonds (black dashed lines) (1) to TPQ hydroxyl group, (2) to second nitrogen of the hydrazine functionality, and (3) to the hydroxyl group of the **2a**. The second nitrogen of **2a** forms a hydrogen bond with TPQ hydroxyl group. (B) The surface rendering of the amino acids closest to **2b** reveals space near C2 of **2b**. The hydrogen bond network (black dashed lines) between TPQ, **2b**, and Asp386 is as tight as in the case of **2a**. The movement of Met211 is not as prominent as in the case of **2a**.

the hydrogen bond between the hydroxyl group of **8** and Asp386 (Figure 4A). Compound **12** forms only two hydrogen bonds: (1) Asp386, the hydroxyl group of TPQ, and (2) Asp386, the hydroxyl group of **12** (Figure 4B). Accordingly, the conformation of **8** is more strongly determined by hydrogen bonding, and these interactions force **8** into a bended conformation. This bended conformation restricts the C2 propyl substituent of **8** from taking advantage of all the extra space created by the rotation of the Met211 side chain. In compound **12**, whose conformation is not strictly determined by hydrogen bonding, the propyl substituent can extend deeper into the extra space (Figure 4). This can be seen as the difference in IC_{50} values between **8** and **12**, which are 1.20 and 0.26 μM, respectively (Table 1).

Effect of Phenyl Substitution at C2. The MD simulations of VAP-1 with bound **2a** and **2b** (Figure 3) and the dockings of **8** and **12** (Figure 4) into VAP-1 clearly show that in compounds **8** and **12**, it is possible to add an even larger substituent than propyl to the C2-position. In the compound series **11**, the C2 substituent is phenyl (R2 in Table 1) while the C1 substituent is methyl (R1 in Table 1), which is the same as in compound **12**. The docking of the **11a** (1*R*, 2*S*) into VAP-1 conformation, obtained in the MD simulation of VAP-1 with bound **2a**,**b**, shows that the phenyl might fit into the VAP-1 ligand-binding site. However, it is difficult to use static protein conformation to predict the binding of other enantiomers of **11**, i.e., **11b**, **11c**, and **11d**. Therefore, to understand the exact binding modes of the enantiomers, we docked all four enantiomers (**11a**—**d**) into a VAP-1 crystal structure[33] where the Leu469 side chain was rotated, as described above, and then the complexes were simulated with MD.

The IC_{50} data of VAP-1 inhibition of **11a**—**d** are intriguing. Although these molecules differ significantly in their stereo configuration, and thus also in their three-dimensional structure, their VAP-1 inhibition potencies show some similarities (**11a** is only 4 times more potent than **11b**) (Table 1). The MD simulations performed for **11a**—**d** bound to VAP-1 indicate two different hydrogen bonding partners for the C1 hydroxyl group, which (1) in **11a** and **11b** form a hydrogen bond to the TPQ (parts A and B of Figure 5, respectively) while (2) in **11c** (Figure 5C) and **11d** (Figure 5D) form a hydrogen bond to the Asp386. Regardless of whether the hydroxyl group of the ligand is hydrogen-bonded with the TPQ or the Asp386, one of the phenyl rings is turned into the hydrophobic pocket formed by Tyr384, Phe389, Tyr394, Leu468, and Leu469 (Figure 5) and the *N*-methyl is pointed toward Ala370. In the conformation in which an intramolecular hydrogen bond with TPQ exists, the phenyl ring at carbon 2 points toward the hydrophobic pocket (**11a** and **11b**, parts A and B of Figure 5). However, with the **11c** and **11d** enantiomers, whose conformation is driven by the

dx.doi.org/10.1021/jm200059p |*J. Med. Chem.* 2011, 54, 2143–2154

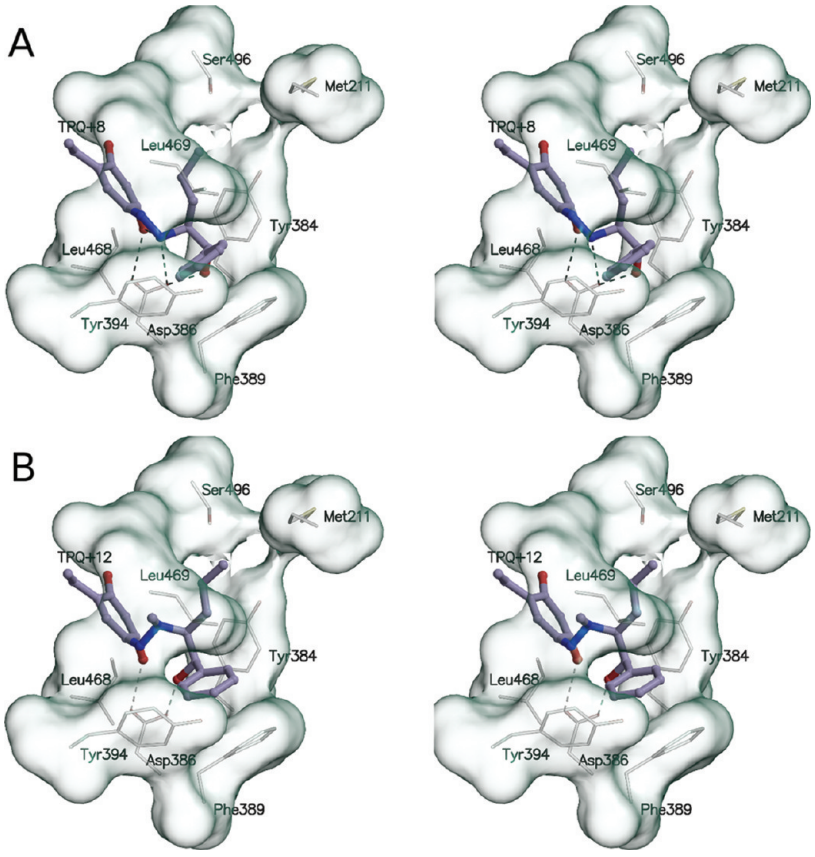

Figure 4. Binding modes of (A) **8** and (B) **12** based on docking simulations to VAP-1 conformation obtained from MD simulations (parallel stereoview). (A) The bound **8** and TPQ are shown in ball-and-stick. A groove formed between Ser496, Met211, and Leu469 can accommodate the C2 substituent. A similar hydrogen bond network is formed as in **2a**. (B) The binding of **12** is distinct to **8** because of the methylation of the second nitrogen atom. Asp386 can form hydrogen bonds to (1) hydroxyl group of **12** and (2) hydroxyl group of TPQ. The phenyl ring of **12** is buried inside the hydrophobic pocket, similar to that in **8**. The propyl substituent extends toward Met211. The *N*-methyl substituent points toward Leu469 main chain. The hydroxyl group of **12** is closer to the hydroxyl group of TPQ than the hydroxyl group of **8**.

hydrogen bonding with the Asp386 (parts C and D of Figure 5), the phenyl ring attached to carbon 1 points toward the hydrophobic pocket. The phenyl ring that is not buried inside the hydrophobic pocket forms a $\pi-\pi$ interaction either with Tyr372 or with Tyr384 (Figure 5).

The conformational changes observed in the MD simulations of VAP-1 with bound inhibitors are predominantly rotational changes in the side chains of the amino acids. The most substantial changes in the conformations of the amino acids in the ligand-binding pocket are related to Met211, Leu469, and TPQ conformations. Interestingly, the conformation of Leu469 seems to be dependent upon the C2 configuration of the ligand. Here, with **11c** and **11d**, the Leu469 returns to the conformation seen in the crystal structure (i.e., to block the ligand-binding cavity[33]). However, with the **11a** and **11b** diastereomers, Leu469 remains in the conformation, where access to the ligand-binding cavity is free. The conformation of Met211 is not dependent upon configurations of C1 and C2. In compounds **11a**−**d**, Met211 turns away from the bound ligand revealing extra space (Figure 5). This is similar to the conformation of Met211 in compounds **2a** and **2b** (Figure 3). The conformation of TPQ also alters on the course of MD simulation, depending upon the C2 configuration of the ligand. With **11c** and **11d**, the TPQ moves to resemble the inactive conformation[34] more than the active conformation.[33] This change in TPQ conformation does not affect the hydrogen-bonding network.

It was expected that the removal of the *N*-methyl from **11** would reduce inhibitory activity, just as it did in the molecule pair **8** and **12**. Indeed, the IC_{50} for **5** is 50 μM, whereas those of **11a**−**d** vary between 0.28 and 1.18 μM (Table 1). Accordingly, N-methylation increases the VAP-1 potency if, simultaneously, C2 has a large substituent. This is interesting because without the C2-substitution the N-methylation has an opposite effect.[26]

VAP-1 over MAO Selectivity. All the compounds evaluated in this study are weak MAO inhibitors showing only a 10-fold variation in MAO inhibition: **2a** (9.90 μM), **2b** (9.80 μM), **8** (11 μM), **11a** (70 μM), **11b** (85 μM), **11c** (99 μM), **11d** (105 μM), **12** (28 μM), and **5** (34 μM). Thus, in general, N-methylated compounds with a phenyl substituent at the R2-position (**11a**−**d**) are slightly worse inhibitors of MAO than those that do not have this type of substituent (**2**, **5**, **8**, and **12**) (Table 1). In contrast, the N-methylation for VAP-1 inhibition has an opposite effect; in this set of compounds, the N-methylation significantly increases the selectivity toward VAP-1 over MAOs (Table 1).

The size of the molecule has a negative effect on the MAO binding (Figure 6) because the ligand-binding pocket in the MAO is smaller than it is in the VAP-1. On the basis of the crystal structure of human MAO B in complex with phenylethylhydrazine, i.e., phenelzine,[45] it can be postulated that both nitrogens of hydrazine moiety are cleaved off during the course of the reaction and the remaining part of the ligand forms a covalent bond with

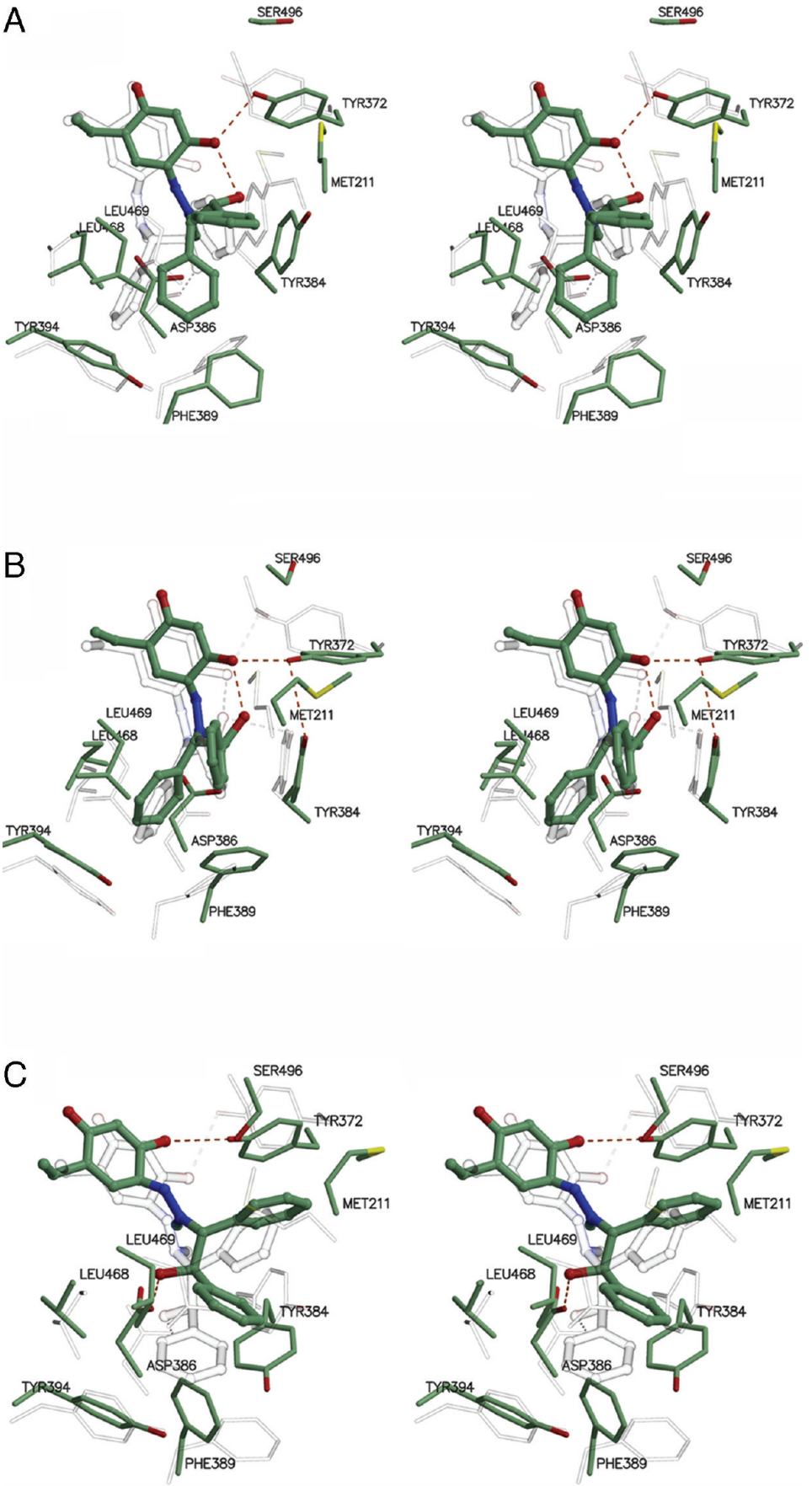

Figure 5. Continued

dx.doi.org/10.1021/jm200059p |*J. Med. Chem.* 2011, 54, 2143–2154

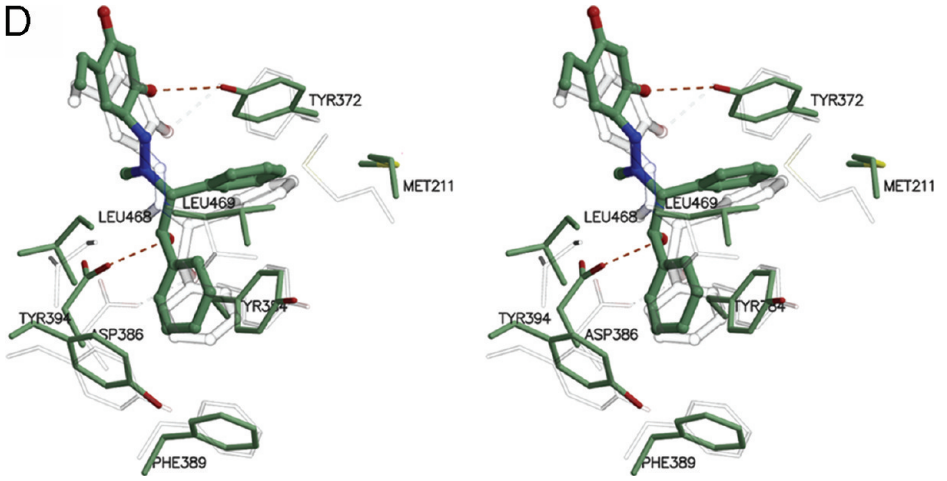

Figure 5. Binding conformations of **11a**−**d** to VAP-1 based on MD simulations (parallel stereoview). Starting structure of VAP-1 MD simulation is visualized in gray and final structure in green. TPQ−ligand complexes and surrounding amino acids are represented in ball-and-sticks and sticks, respectively. Hydrogen bonds in MD starting structure are drawn with dotted black line, and those in MD final structure are drawn with dotted orange line. All main chain atoms are omitted. (A) The binding of **11a** to VAP-1. In the MD simulation starting structure the ligand forms hydrogen bond with Asp386. In the final structure the ligand OH group has moved markedly. This change recruits Tyr372 and Tyr384 to form hydrogen bonds that were initially absent, resembling the final structure of the **11b**. (B) Binding of **11b** to VAP-1. The ligand has formed a hydrogen bond with the TPQ OH group. The surrounding tyrosines Tyr372 and Tyr384 also form hydrogen bonds to the ligand and TPQ. Tyr372 changes its conformation during the simulation, and in the final structure it is close enough to be hydrogen-bonded to Tyr384. The overall conformation of the ligand does not change markedly. (C) Binding of **11c** to VAP-1. Ligand OH group forms a hydrogen bond with Asp386. Surrounding aromatic amino acids (Tyr372, Tyr384, and Phe389) undergo conformational changes during simulation as the ligand moves. TPQ moves toward the protein core. (D) Binding of **11d** to VAP-1. The ligand is hydrogen-bonded to the Asp386 throughout the simulation. The TPQ−ligand complex moves slightly toward the protein core. A hydrogen bond between Tyr372 and TPQ OH group can be detected.

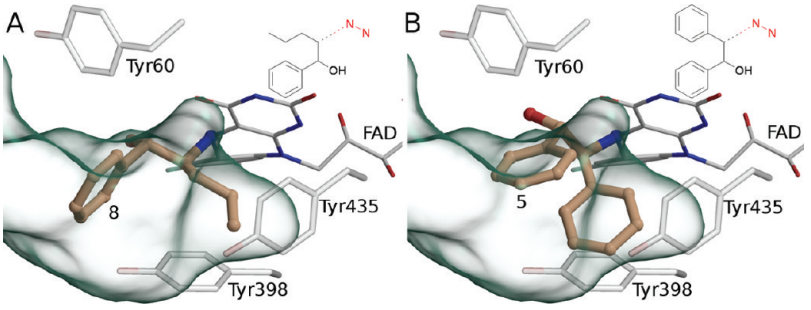

Figure 6. Binding of **5** and **8** into MAO B ligand binding site. The ligand binding pocket of MAO is small and narrow (represented as green surface). The ligands, **5** and **8**, are covalently docked to the nitrogen of cofactor FAD and are represented as ball-and-sticks. The reaction product of **8** (A) fits slightly better into the ligand binding pocket of MAO than that of **5** (B), thus explaining their difference in inhibitor potency to MAO. The surrounding tyrosines, Tyr60, Tyr398, and Tyr435, of the ligand binding pocket are shown as transparent ball-and-sticks.

the nitrogen atom at the central ring of the FAD. The docking simulations of the probable covalent reaction product of **8** (1-phenyl-2-propanylethanol, Figure 6A) and **5** (1,2-diphenylethanol, Figure 6B) to MAO B indicate that the MAO ligand-binding site is too small to properly accommodate these compounds. Furthermore, the MAO ligand-binding site is too small to accommodate compounds **11a**−**d** (data not shown). However, it is notable that the propyl group of **8**, at R2-position, fits slightly better into the MAO ligand-binding site (Figure 6A), possibly explaining the small difference in their potency (Table 1). Additionally, the docking of **8** into the MAO ligand-binding site is easier because of the flexibility of the propyl group in contrast to the phenyl group in **5**.

The negative effect of N-methylation on MAO binding may be explained by the lowered reactivity of the N-methylated molecules compared to the reactivity of the nonsubstituted molecules. Even though molecules **8** and **12** yield the same reaction product in MAO, N-methylated compound **12** has only half of the inhibition activity for MAO than does compound **8**, which is not N-methylated (Table 1). Similarly, non-N-methylated compound **5** has twice the potency to MAO than do the N-methylated compounds **11a**−**d** (Table 1).

CONCLUSIONS

This study has explored the flexibility of the VAP-1 ligand-binding site and developed several novel VAP-1 selective inhibitors over MAO. The MD simulations show that the static crystal structures of VAP-1 provide only a limited view into

ligand-binding capability. The VAP-1 ligand-binding site can accommodate bulkier inhibitors than can MAO. Additionally, the N-methylation of large hydrazines increases the potency of VAP-1 while the inhibition of MAO is simultaneously reduced, thus leading to VAP-1 selectivity. Altogether, these findings open up new avenues into the discovery of novel and selective inhibitors to treat diseases related to VAP-1.

MATERIALS AND METHODS

Materials. Cell culture reagents were supplied by Gibco. Other chemicals were of analytical or reagent grade and were purchased from commercial suppliers.

Synthesis of the Novel Hydrazine-like Molecules. *General Methods.* Melting points were measured on a Kofler hot-plate microscope apparatus and are uncorrected. For routine thin-layer chromatography (TLC), silica gel 60 F_{254} plates (Merck, Germany) were used. Elemental analyses were performed with a Perkin-Elmer 2400 CHNS elemental analyzer. ^{1}H NMR spectra were recorded in $CDCl_3$, in DMSO-d_6, or in D_2O solutions on a Bruker DRX 400 spectrometer. These spectra indicated the >95% purities of the prepared compounds. Chemical shifts are given in δ (ppm) relative to TMS (DMSO-d_6) or to TSP (D_2O) as internal standards.

General Procedure for the Preparation of Hydrazino Alcohols ***2a,b***. To a stirred solution of hydrazine hydrate (5.01 g, 0.10 mol) in EtOH (10 mL) a solution of (*R*)- or (*S*)-styrene oxide (**1a** or **1b**, 1.20 g, 10 mmol) in EtOH (5 mL) was added dropwise. After addition was complete, the mixture was kept at 60 °C for 10 min. The solvent was evaporated off, and the oily residue was dissolved in EtOH and treated with an equivalent amount of maleic acid. The separated crystals of the corresponding maleates (**2a,b**) were filtered off and recrystallized.

*(R)-2-Hydrazino-1-phenylethanol Hydrogen Maleate (**2a** Hydrogen Maleate).* Beige crystalline solid; yield 1.45 g (54%); mp 98−103 °C (EtOH−Et_2O); $[\alpha]_D$ −44 (MeOH, *c* 0.50). ^{1}H NMR (D_2O) δ 3.38 (m, 2H, *J* = 7.9 Hz, NCH_2), 5.07 (dd, 1H, *J* = 7.1, 5.7 Hz, OC*H*), 6.30 (s, 2H, C*H*═C*H*), 7.38−7.50 (m, 5H, C_6H_5). Anal. Calcd for $C_{12}H_{16}N_2O_5$: C, 53.73; H, 6.01; N, 10.44. Found: C, 53.51; H, 5.93; N, 10.28.

*(S)-2-Hydrazino-1-phenylethanol Hydrogen Maleate (**2b** Hydrogen Maleate).* Beige crystalline solid; yield 1.40 g (52%); mp 99−104 °C (EtOH−Et_2O); $[\alpha]_D$ +43 (MeOH, *c* 0.50). The ^{1}H NMR (D_2O) spectrum was identical to that of the (*R*)-enantiomer (**2a** hydrogen maleate). Anal. Calcd for $C_{12}H_{16}N_2O_5$: C, 53.73; H, 6.01; N, 10.44. Found: C, 53.64; H, 5.85; N, 10.38.

(1R,2R*)-2-Hydrazino-1,2-diphenylethanol Hydrogen Maleate (**5** Hydrogen Maleate).* To a solution of (±)-*trans*-stilbene oxide (**4**, 1.57 g, 8 mmol) in EtOH (10 mL) hydrazine hydrate (5.01 g, 100 mmol) was added. The mixture was heated under reflux for 12 h. The solvent and the unreacted hydrazine hydrate were evaporated off, and evaporation was repeated twice after addition of toluene (10 mL). The oily residue was treated with an equivalent amount of maleic acid in a mixture of EtOH and Et_2O to give crystalline maleate salt which was filtered off and recrystallized. White crystalline substance; yield 1.71 g (62%); mp 159−160 °C (EtOH−Et_2O). ^{1}H NMR (D_2O) δ (ppm): 4.41 (d, 1H, *J* = 6.5 Hz, NC*H*), 5.10 (d, 1H, *J* = 6.5 Hz, OC*H*), 6.30 (s, 2H, C*H*COOH) 7.28−7.49 (m, 10H, 2 × C_6H_5). Anal. Calcd for $C_{18}H_{20}N_2O_5$: C, 62.78; H, 5.85; N, 8.13. Found: C, 62.50; H, 5.67; N, 7.96.

*2-Hydrazino-1-phenylpentanol Hydrogen Fumarate (**8** Hydrogen Fumarate).* To a stirred and ice-cooled solution of (±)-2-bromo-1-phenyl-1-pentanone (**6**, 2.41 g, 10 mmol) in methanol (30 mL) $NaBH_4$ (0.38 g, 10 mmol) was added in small portions, and the resulting mixture was stirred for 2 h with ice−water bath. The mixture was then acidified with 10% HCl and evaporated in vacuo. The residue was partitionated between water (30 mL) and Et_2O (25 mL), and the aqueous phase was extracted with Et_2O (2 × 25 mL). The combined organic phases were dried (Na_2SO_4) and evaporated to give compound **7** as an oily product which was used in the next step without further purification. Yield: 2.42 g (∼100%).

To a solution of compound **7** (2.42 g, 10 mmol) in ethanol (30 mL) hydrazine hydrate (2.50 g, 50 mmol) was added, and the mixture was heated under reflux for 6 h. The solvent and the unreacted hydrazine hydrate were evaporated off, and evaporation was repeated twice after addition of toluene (10 mL). The oily residue was treated with an equivalent amount of fumaric acid in a mixture of EtOH and Et_2O to give crystalline fumarate salt which was filtered off and recrystallized. Beige crystalline substance; yield 1.64 g (53%); mp 170 °C (decomposition) (EtOH−Et_2O). ^{1}H NMR (DMSO-d_6) δ (ppm): 0.68 (t, 3H, *J* = 7.0 Hz, CH_3), 0.94−1.36 (m, 4H, 2 × CH_2), 2.80−2.91 (m, 1H, NC*H*), 4.53 (d, 1H, *J* = 8.2 Hz, OC*H*), 6.51 (s, 2H, C*H*COOH), 7.16−7.42 (m, 5H, C_6H_5). Anal. Calcd for $C_{15}H_{22}N_2O_5$: C, 58.05; H, 7.15; N, 9.03. Found: C, 57.75; H, 6.94; N, 8.89.

General Procedure for the Preparation of N-Nitrosoamino Alcohols ***10a−d***. A solution of $NaNO_2$ (1.38 g, 20 mmol) in H_2O (10 mL) was added dropwise to a suspension of the corresponding isomer of 2-methylamino-1,2-diphenyl-1-ethanol (**7a−d**, 2.27 g, 10 mmol) (10 mmol) in H_2O (25 mL) with vigorous stirring on an ice-cold bath, and then AcOH (0.90 g, 15 mmol) was added dropwise. The mixture was stirred at room temperature for 8 h, then was extracted with EtOAc (4 × 30 mL). The combined organic phases were dried (Na_2SO_4) and evaporated under reduced pressure to give the *N*-nitroso derivative as a crystalline product, which was filtered and washed with *n*-hexane. Yield: 2.44−2.49 g (95−97%). The crude product was used in the next step without further purification.

General Procedure for the Preparation of Hydrazino Alcohols ***11a−d***. A solution of the corresponding isomer of 2-methylamino-*N*-nitroso-1,2-diphenyl-1-ethanol (**10a−d**, 1.54 g, 6 mmol) in THF (12 mL) was added dropwise to a stirrred and ice-cooled suspension of $LiAlH_4$ (0.46 g, 12 mmol) in THF (25 mL), and the mixture was stirred at ambient temperature for 3 h. The excess of $LiAlH_4$ was decomposed with a mixture of H_2O (1.0 mL) and THF (20 mL). The resulting precipitate was filtered off and washed with EtOAc (3 × 25 mL). The combined filtrate and washings were dried (Na_2SO_4) and evaporated under reduced pressure. The oily residue was treated with an equivalent amount of fumaric acid (**11b,c**) or (*S,S*)-tartaric acid (**11a,d**) in a mixture of EtOH and Et_2O to give crystalline salts which was filtered off and recrystallized. The salt formations of **11b** and **11c** with fumaric acid occurred in 1:1 ratio, while tartrates of **11a** and **11d** could be characterized by the 2:1 ratios of the base and acid components.

*(1R,2S)-2-(1-Methylhydrazino)-1,2-diphenylethanol (S,S)-Tartrate [**11a** (S,S)-Tartrate].* White crystalline substance; yield 1.10 g (58%); mp 141−143 °C (EtOH−Et_2O); $[\alpha]_D$ −85 (MeOH, *c* 0.57). ^{1}H NMR (D_2O) δ (ppm): 2.95 (s, 3H, NCH_3), 4.35 (s, 1H, C*H*OHCOOH), 4.45 (d, 1H, *J* = 4.8 Hz, NC*H*), 5.67 (d, 1H, *J* = 4.8 Hz, OC*H*), 7.18−7.46 (m, 10H, 2 × C_6H_5). Anal. Calcd for $C_{17}H_{21}N_2O_4$: C, 64.34; H, 6.67; N, 8.83. Found: C, 64.28; H, 6.31; N, 8.99.

*(1S,2S)-2-(1-Methylhydrazino)-1,2-diphenylethanol Hydrogen Fumarate (**11b** Hydrogen Fumarate).* White crystalline substance; yield 1.33 g (62%); mp 153−154 °C (EtOH−Et_2O); $[\alpha]_D$ −44 (MeOH, *c* 0.40). ^{1}H NMR (D_2O) δ (ppm): 2.83 (s, 3H, NCH_3), 4.62 (d, 1H, *J* = 10.3 Hz, NC*H*), 5.43 (d, 1H, *J* = 10.3 Hz, OC*H*), 6.60 (s, 2H, C*H*COOH), 7.10−7.46 (m, 10H, 2 × C_6H_5). Anal. Calcd for $C_{19}H_{22}N_2O_5$: C, 63.67; H, 6.19; N, 7.82. Found: C, 63.68; H, 5.93; N, 7.66.

*(1R,2R)-2-(1-Methylhydrazino)-1,2-diphenylethanol Hydrogen Fumarate (**11c** Hydrogen Fumarate).* White crystalline substance; yield 1.40 g (65%); mp 150−152 °C (EtOH−Et_2O); $[\alpha]_D$ +41 (MeOH, *c* 0.40). The ^{1}H NMR (D_2O) spectrum was identical to that of the (1*S*,2*S*)

enantiomer (**11b** hydrogen fumarate). Anal. Calcd for $C_{19}H_{22}N_2O_5$: C, 63.67; H, 6.19; N, 7.82. Found: C, 63.45; H, 6.08; N, 7.71.

*(1S,2R)-2-(1-Methylhydrazino)-1,2-diphenylethanol (S,S)-Tartrate [**11d** (S,S)-Tartrate].* White crystalline substance; yield 1.24 g (65%); mp 167−170 °C (EtOH−Et_2O); $[\alpha]_D$ +78 (MeOH, *c* 0.55). ^{1}H NMR (D_2O) δ (ppm): 2.94 (s, 3H, NCH_3), 4.35 (s, 1H, C*H*OHCOOH), 4.44 (d, 1H, *J* = 4.9 Hz, NC*H*), 5.66 (d, 1H, *J* = 4.9 Hz, OC*H*), 7.18−7.46 (m, 10H, 2 × C_6H_5). Anal. Calcd for $C_{17}H_{21}N_2O_4$: C, 64.34; H, 6.67; N, 8.83. Found: C, 64.07; H, 6.48; N, 8.51.

Expression of Recombinant VAP-1. Recombinant VAP-1 protein was obtained from Chinese hamster ovary (CHO) cells stably transfected with a full-length human VAP-1 cDNA. Recombinant human VAP-1 SSAO expressed in CHO cells was used as a source of VAP-1 for activity measurements. Native CHO cells have negligible VAP-1 activity. These cells and their culture have previously been described.[46] A cell lysate was prepared by suspending approximately 3.6×10^8 cells in 25 mL of lysis buffer (150 mM NaCl, 10 mM Tris base, pH 7.2, 1.5 mM $MgCl_2$, 1% NP40) and incubating at 4 °C overnight on a rotating table. The lysate was clarified by centrifugation at 18000*g* for 5 min at room temperature and the supernatant used directly in the assay.

Mitochondrial MAO Extract. Rat total monoamine oxidase enzyme (MAO, mixture of MAO A and MAO B) was prepared from rat liver tissues by rinsing the liver sample several times in KCl−EDTA solution to remove all blood. Then the liver sample was homogenized in ice-cold potassium phosphate buffer (0.1 M, pH 7.4) with an Ultra-Turax homogenizer (setting 11 000 rpm, 4 × 10 s). After centrifugation at 500*g* for 10 min at 4 °C the supernatant was carefully withdrawn and was centrifuged at 12300*g* for 15 min at 4 °C. The supernatant was discharged, and sedimented mitochondria were resuspended in fresh phosphate buffer and centrifuged as previously. The mitochondria were suspended in phosphate buffer and homogenized with an Ultra-Turax homogenizer (setting 11 000 rpm, 2 × 10 s). Mitochondrial preparate was aliquoted and stored at −70 °C.

In Vitro Inhibition Activity. VAP-1 activity was measured as described previously[26] using the coupled colorimetric method essentially as described for monoamine oxidase and related enzymes.[47] In short, the assay was performed in 96-well microtiter plates as follows. The inhibitor concentrations used varied between 1 nM and 50 μM. The assay was performed in a final volume of 200 μL consisting of 0.2 M potassium phosphate buffer (pH 7.6) and freshly made chromogenic solution containing 1 mM 2,4-dichlorophenol, 500 μM 4-aminoantipyrine, and 4 U/mL horseradish peroxidase and an amount of CHO cell lysate containing VAP-1 SSAO that caused a change of 0.6A_{490} per h. The plates were incubated for 30 min at 37 °C. To initiate the enzymatic reaction, 1 mM benzylamine was added and the plate incubated for 1 h at 37 °C. The increase in absorbance, reflecting VAP-1 SSAO activity, was measured at 490 nm by using Wallac Victor II multilabel counter. The IC_{50} values for the inhibitors were calculated using GraphPad Prism software. Since MAO A and MAO B have similar amino acids at the proposed inhibitor binding site (Figure 6), the IC_{50} values for MAOs were measured only for the mixture of MAO A and MAO B. Total MAO activity was measured in a similar way as for VAP-1 SSAO except that 2,4-dichlorophenol was replaced by 1 mM vanillic acid, and benzylamine was replaced by tyramine in 0.5 mM final concentration.

Docking of Ligands to VAP-1 and MAO B Ligand Binding Pockets. The crystal structure of VAP-1 in complex with 2-hydrazinopyridine[33] was retrieved from the Protein Data Bank.[48] The conformation of the side chain of Leu469 was changed to resemble that obtained from MD simulations[26] using amino acid side chain rotamer library[49] incorporated into BODIL modeling environment.[50] In addition, the water molecules and the atoms of bound inhibitor molecule 2-hydrazinopyridine (C1, C2, C3, C4, C5, and N3 in the crystal structure) were removed. Hydrogen atoms were added using SYBYL.[51] Ligands were sketched in SYBYL and energy-minimized by using MMFF94s force field with MMFF94 charges and conjugate gradient method until the energy gradient was less than 0.05 kcal/mol. Bioactive conformations for studied ligands were predicted with GOLD 3.1.1. The ligand binding pocket was defined using the C^{β}H from Leu468 as a central atom with radius of 20 Å. The ligands were docked covalently to TPQ. Each ligand was docked 10 times; however, the docking simulation was allowed to terminate in cases where the root-mean-squared deviations of the three best conformations were within 1.5 Å. Compounds **5**, **8**, and **12** were docked on the final conformation of the MD simulation of VAP-1 with **2a** instead of the modified crystal structure of VAP-1 described above. Docking of ligands into crystal structures of MAO A[52] and MAO B[45] was performed with GOLD 3.1.1 similarly as docking to VAP-1. Molecules were docked covalently to the nitrogen atom of cofactor FAD.

Starting Structures for Molecular Dynamics Simulations. The starting structure of VAP-1 with an active conformation of cofactor TPQ[32] was retrieved from the Protein Data Bank.[48] Leu469 side chain was turned as described earlier.[26] As all studied inhibitor molecules bind covalently to TPQ, the TPQ−ligand systems were parametrized as follows. TPQ−ligand complexes were built with SYBYL 7.3[51] and optimized with Gaussian 03[53] at the HF/6-31+G* level. The electrostatic potentials of the ligands were calculated with Gaussian 03 (HF/6-31+G*) for the optimized TPQ−ligand complexes, and the RESP methodology[54] was used to create atom-centered point charges from the electrostatic potentials. Finally, hydrogens, neutralizing counterions (Na^+ ions), and TIP3P water molecules extending 13 Å around the protein complex (rectangular box) were added with LEAP.[55]

Molecular Dynamics Simulations. All energy minimizations and molecular dynamics simulations were performed with NAMD 2.6[56] using ff03 force field parameters[57] for the protein and gaff99 parameters[58] for the ligands (TPQ + compounds **2a**,**b** and **11a**−**d**). The whole MD simulation procedure comprised two minimization runs (the minimization of water molecules, counterions, and amino acid side chains, followed by the minimization for the whole complex) and two MD simulations. The first MD simulation (360 ps) where the Cα atoms were restrained was performed at constant pressure. The 2.4 ns production simulation was performed without constraints. The simulated complexes were held at constant temperature (300 K) with Langevin dynamics for all non-hydrogen atoms, using a Langevin damping coefficient of 5 ps^{-1}. A constant pressure of 1 atm was upheld by a Nosé−Hoover−Langevin piston[59] with an oscillation time scale of 200 fs and a damping time scale of 100 fs. An integration time step of 2 fs was used under a multiple time stepping scheme.[60] The bonded and short-range interactions were calculated every third step. A cutoff value of 12 Å was used for the van der Waals and short-range van der Waals forces to smoothen the cutoff. The simulations were conducted under the periodic boundary conditions with the full system, and the long-range electrostatics were counted with the particle-mesh Ewald method.[61] The bonds involving hydrogen atoms were restrained by the SHAKE algorithm.[62] Snapshot structures from the MD trajectories were visually inspected to understand the potencies and effects of inhibitors to the structure of the catalytic site.

AUTHOR INFORMATION

Corresponding Author

*Phone: +358-40-521-6913. Fax: +358-14-260-2221. E-mail: olli.t.pentikainen@jyu.fi.

ACKNOWLEDGMENT

This study was financially supported by Academy of Finland (Grant 121393 for U.P. and Grant 129175 for O.T.P.). CSC-Finnish IT Center for Science is thanked for generous computational grant (Grant jyy2516 for O.T.P.).

■ ABBREVIATIONS USED

VAP-1, vascular adhesion protein-1; MAO, monoamine oxidase; AO, amine oxidase; MD, molecular dynamics; TPQ, topaquinone

■ REFERENCES

(1) Marttila-Ichihara, F.; Smith, D. J.; Stolen, C.; Yegutkin, G. G.; Elima, K.; Mercier, N.; Kiviranta, R.; Pihlavisto, M.; Alaranta, S.; Pentikäinen, U.; Pentikäinen, O.; Fülöp, F.; Jalkanen, S.; Salmi, M. Vascular amine oxidases are needed for leukocyte extravasation into inflamed joints in vivo. *Arthritis Rheum.* **2006**, *54*, 2852–2862.

(2) Salmi, M.; Kalimo, K.; Jalkanen, S. Induction and function of vascular adhesion protein-1 at sites of inflammation. *J. Exp. Med.* **1993**, *178*, 2255–2260.

(3) Zorzano, A.; Abella, A.; Marti, L.; Carpene, C.; Palacin, M.; Testar, X. Semicarbazide-sensitive amine oxidase activity exerts insulin-like effects on glucose metabolism and insulin-signaling pathways in adipose cells. *Biochim. Biophys. Acta* **2003**, *1647*, 3–9.

(4) Mathys, K. C.; Ponnampalam, S. N.; Padival, S.; Nagaraj, R. H. Semicarbazide-sensitive amine oxidase in aortic smooth muscle cells mediates synthesis of a methylglyoxal-AGE: implications for vascular complications in diabetes. *Biochem. Biophys. Res. Commun.* **2002**, *297*, 863–869.

(5) Madej, A.; Reich, A.; Orda, A.; Szepietowski, J. C. Expression of vascular adhesion protein-1 in atopic eczema. *Int. Arch. Allergy Immunol.* **2006**, *139*, 114–121.

(6) Madej, A.; Reich, A.; Orda, A.; Szepietowski, J. C. Vascular adhesion protein-1 (VAP-1) is overexpressed in psoriatic patients. *J. Eur. Acad. Dermatol. Venereol.* **2007**, *21*, 72–78.

(7) Olive, M.; Unzeta, M.; Moreno, D.; Ferrer, I. Overexpression of semicarbazide-sensitive amine oxidase in human myopathies. *Muscle Nerve* **2004**, *29*, 261–266.

(8) Jiang, Z. J.; Richardson, J. S.; Yu, P. H. The contribution of cerebral vascular semicarbazide-sensitive amine oxidase to cerebral amyloid angiopathy in Alzheimer's disease. *Neuropathol. Appl. Neurobiol.* **2008**, *34*, 194–204.

(9) Ferrer, I.; Lizcano, J. M.; Hernandez, M.; Unzeta, M. Over-expression of semicarbazide sensitive amine oxidase in the cerebral blood vessels in patients with Alzheimer's disease and cerebral autosomal dominant arteriopathy with subcortical infarcts and leukoencephalopathy. *Neurosci. Lett.* **2002**, *321*, 21–24.

(10) Airas, L.; Mikkola, J.; Vainio, J. M.; Elovaara, I.; Smith, D. J. Elevated serum soluble vascular adhesion protein-1 (VAP-1) in patients with active relapsing remitting multiple sclerosis. *J. Neuroimmunol.* **2006**, *177*, 132–135.

(11) Kurkijärvi, R.; Adams, D. H.; Leino, R.; Mottonen, T.; Jalkanen, S.; Salmi, M. Circulating form of human vascular adhesion protein-1 (VAP-1): increased serum levels in inflammatory liver diseases. *J. Immunol.* **1998**, *161*, 1549–1557.

(12) Roessner, V.; Weber, A.; Becker, A.; Beck, G.; Kornhuber, J.; Frieling, H.; Bleich, S. Decreased serum semicarbazide sensitive aminooxidase (SSAO) activity in patients with major depression. *Prog. Neuro-Psychopharmacol. Biol. Psychiatry* **2006**, *30*, 906–909.

(13) Forster-Horvath, C.; Dome, B.; Paku, S.; Ladanyi, A.; Somlai, B.; Jalkanen, S.; Timar, J. Loss of vascular adhesion protein-1 expression in intratumoral microvessels of human skin melanoma. *Melanoma Res.* **2004**, *14*, 135–140.

(14) Jaakkola, K.; Kaunismäki, K.; Tohka, S.; Yegutkin, G.; Vänttinen, E.; Havia, T.; Pelliniemi, L. J.; Virolainen, M.; Jalkanen, S.; Salmi, M. Human vascular adhesion protein-1 in smooth muscle cells. *Am. J. Pathol.* **1999**, *155*, 1953–1965.

(15) Toiyama, Y.; Miki, C.; Inoue, Y.; Kawamoto, A.; Kusunoki, M. Circulating form of human vascular adhesion protein-1 (VAP-1): decreased serum levels in progression of colorectal cancer and predictive marker of lymphatic and hepatic metastasis. *J. Surg. Oncol.* **2009**, *99*, 368–372.

(16) Roessner, V.; Weber, A.; Becker, A.; Beck, G.; Frieling, H.; Bleich, S. Decreased serum activity of semicarbazide-sensitive amine oxidase (SSAO) in patients treated with second generation antipsychotics: a link to impaired glucose metabolism?. *Eur. J. Clin. Pharmacol.* **2007**, *63*, 425–429.

(17) Boomsma, F.; Bhaggoe, U. M.; van der Houwen, A. M.; van den Meiracker, A. H. Plasma semicarbazide-sensitive amine oxidase in human (patho)physiology. *Biochim. Biophys. Acta* **2003**, *1647*, 48–54.

(18) Boomsma, F.; Derkx, F. H.; van den Meiracker, A. H.; Man in't Veld, A. J.; Schalekamp, M. A. Plasma semicarbazide-sensitive amine oxidase activity is elevated in diabetes mellitus and correlates with glycosylated haemoglobin. *Clin. Sci. (London)* **1995**, *88*, 675–679.

(19) Garpenstrand, H.; Ekblom, J.; Backlund, L. B.; Oreland, L.; Rosenqvist, U. Elevated plasma semicarbazide-sensitive amine oxidase (SSAO) activity in type 2 diabetes mellitus complicated by retinopathy. *Diabetic Med.* **1999**, *16*, 514–521.

(20) Kurkijärvi, R.; Jalkanen, S.; Isoniemi, H.; Salmi, M. Vascular adhesion protein-1 (VAP-1) mediates lymphocyte−endothelial interactions in chronic kidney rejection. *Eur. J. Immunol.* **2001**, *31*, 2876–2884.

(21) Weiss, H. G.; Klocker, J.; Labeck, B.; Nehoda, H.; Aigner, F.; Klingler, A.; Ebenbichler, C.; Foger, B.; Lechleitner, M.; Patsch, J. R.; Schwelberger, H. G. Plasma amine oxidase: a postulated cardiovascular risk factor in nondiabetic obese patients. *Metabolism* **2003**, *52*, 688–692.

(22) Boomsma, F.; van Veldhuisen, D. J.; de Kam, P. J.; Man in't Veld, A. J.; Mosterd, A.; Lie, K. I.; Schalekamp, M. A. Plasma semicarbazide-sensitive amine oxidase is elevated in patients with congestive heart failure. *Cardiovasc. Res.* **1997**, *33*, 387–391.

(23) Wang, E. Y.; Gao, H.; Salter-Cid, L.; Zhang, J.; Huang, L.; Podar, E. M.; Miller, A.; Zhao, J.; O'Rourke, A.; Linnik, M. D. Design, synthesis, and biological evaluation of semicarbazide-sensitive amine oxidase (SSAO) inhibitors with anti-inflammatory activity. *J. Med. Chem.* **2006**, *49*, 2166–2173.

(24) Yabanoglu, S.; Ucar, G.; Gokhan, N.; Salgin, U.; Yesilada, A.; Bilgin, A. A. Interaction of rat lung SSAO with the novel 1-N-substituted thiocarbamoyl-3-substituted phenyl-5-(2-pyrolyl)-2-pyrazoline derivatives. *J. Neural Transm.* **2007**, *114*, 769–773.

(25) Olarte, A. Z.; Mian, A.; Clauzel, L. M.; Exposito, M. R.; Font, F. Y.; Palomera, F. A. WO 2006013209, 2006.

(26) Nurminen, E. M.; Pihlavisto, M.; Lázár, L.; Szakonyi, Z.; Pentikäinen, U.; Fülöp, F.; Pentikäinen, O. T. Synthesis, in vitro activity, and three-dimensional quantitative structure−activity relationship of novel hydrazine inhibitors of human vascular adhesion protein-1. *J. Med. Chem.* **2010**, *53*, 6301–6315.

(27) Olivieri, A.; Tipton, K.; O'Sullivan, J. L-Lysine as a recognition molecule for the VAP-1 function of SSAO. *J. Neural Transm.* **2007**, *114*, 747–749.

(28) Yegutkin, G. G.; Salminen, T.; Koskinen, K.; Kurtis, C.; McPherson, M. J.; Jalkanen, S.; Salmi, M. A peptide inhibitor of vascular adhesion protein-1 (VAP-1) blocks leukocyte-endothelium interactions under shear stress. *Eur. J. Immunol.* **2004**, *34*, 2276–2285.

(29) Wang, X.; Pietrangeli, P.; Mateescu, M. A.; Mondovi, B. Extended substrate specificity of serum amine oxidase: possible involvement in protein posttranslational modification. *Biochem. Biophys. Res. Commun.* **1996**, *223*, 91–97.

(30) Kirton, C. M.; Laukkanen, M. L.; Nieminen, A.; Merinen, M.; Stolen, C. M.; Armour, K.; Smith, D. J.; Salmi, M.; Jalkanen, S.; Clark, M. R. Function-blocking antibodies to human vascular adhesion protein-1: a potential anti-inflammatory therapy. *Eur. J. Immunol.* **2005**, *35*, 3119–3130.

(31) Jalkanen, S.; Jalkanen, M.; Salmi, M. WO/2006/134203, 2006.

(32) Jakobsson, E.; Nilsson, J.; Kallstrom, U.; Ogg, D.; Kleywegt, G. J. Crystallization of a truncated soluble human semicarbazide-sensitive amine oxidase. *Acta Crystallogr., Sect. F: Struct. Biol. Cryst. Commun.* **2005**, *61*, 274–278.

(33) Jakobsson, E.; Nilsson, J.; Ogg, D.; Kleywegt, G. J. Structure of human semicarbazide-sensitive amine oxidase/vascular adhesion

protein-1. *Acta Crystallogr., Sect. D: Biol. Crystallogr.* **2005**, *61*, 1550–1562.

(34) Airenne, T. T.; Nymalm, Y.; Kidron, H.; Smith, D. J.; Pihlavisto, M.; Salmi, M.; Jalkanen, S.; Johnson, M. S.; Salminen, T. A. Crystal structure of the human vascular adhesion protein-1: unique structural features with functional implications. *Protein Sci.* **2005**, *14*, 1964–1974.

(35) Wilmot, C. M.; Murray, J. M.; Alton, G.; Parsons, M. R.; Convery, M. A.; Blakeley, V.; Corner, A. S.; Palcic, M. M.; Knowles, P. F.; McPherson, M. J.; Phillips, S. E. Catalytic mechanism of the quinoenzyme amine oxidase from *Escherichia coli*: exploring the reductive half-reaction. *Biochemistry* **1997**, *36*, 1608–1620.

(36) Mure, M.; Kurtis, C. R.; Brown, D. E.; Rogers, M. S.; Tambyrajah, W. S.; Saysell, C.; Wilmot, C. M.; Phillips, S. E.; Knowles, P. F.; Dooley, D. M.; McPherson, M. J. Active site rearrangement of the 2-hydrazinopyridine adduct in *Escherichia coli* amine oxidase to an azo copper(II) chelate form: a key role for tyrosine 369 in controlling the mobility of the TPQ-2HP adduct. *Biochemistry* **2005**, *44*, 1583–1594.

(37) Zalan, Z.; Lázár, L.; Fülöp, F. Chemistry of hydrazinoalcohols and their heterocyclic derivatives. Part 1. Synthesis of hydrazinoalcohols. *Curr. Org. Chem.* **2005**, *9*, 357–376.

(38) Kim, M.; White, J. D. Olefins from thermal decomposition of *N*-sulfoximino-2-oxazolidones. A novel synthesis of bicyclo[3.3.1]non-1-ene. *J. Am. Chem. Soc.* **1977**, *99*, 1172–1180.

(39) Biel, J. H.; Drukker, A. E.; Mitchell, T. F.; Sprengeler, E. P.; Nuhfer, P. A.; Conway, A. C.; Horita, A. Central stimulants. Chemistry and structure−activity relationship of aralkyl hydrazines. *J. Am. Chem. Soc.* **1959**, *81*, 2805–2813.

(40) Meltzer, P. C.; Butler, D.; Deschamps, J. R.; Madras, B. K. 1-(4-Methylphenyl)-2-pyrrolidin-1-yl-pentan-1-one (pyrovalerone) analogues: a promising class of monoamine uptake inhibitors. *J. Med. Chem.* **2006**, *49*, 1420–1432.

(41) Amschler, U.; Schultz, O. Halogen-analoge des adrenalins und isoproterenols. *Arzneim.-Forsch./Drug Res.* **1972**, *22*, 2095–2096.

(42) Wheatley, W. B.; Fitzgibbon, W. E.; Cheney, L. C. 1,2-Diphenyl-2-aminoethanols. I. Synthesis of some erythro-1,2-diphenyl-2-alkylaminoethanols. *J. Org. Chem.* **1953**, *18*, 1564–1571.

(43) Takahashi, H.; Tomita, K.; Noguchi, H.; Otomasu, H. Absolute configuration of (+)-erythro-2-methylamino-1,2-diphenylethanol and asymmetric synthesis by using its chirality. *J. Pharm. Soc. Jpn.* **1979**, *99* (3), 280–284.

(44) Lou, R.; Mi, A.; Jiang, Y.; Qin, Y.; Li, Z.; Fu, F.; Chan, A. S. C. Aminophosphine phosphinites derived from chiral 1,2-diphenyl-2-aminoethanols: synthesis and application in rhodium-catalyzed asymmetric hydrogenation of dehydroamino acid derivatives. *Tetrahedron* **2000**, *56*, 5857–5863.

(45) Binda, C.; Wang, J.; Li, M.; Hubalek, F.; Mattevi, A.; Edmondson, D. E. Structural and mechanistic studies of arylalkylhydrazine inhibition of human monoamine oxidases A and B. *Biochemistry* **2008**, *47*, 5616–5625.

(46) Smith, D. J.; Salmi, M.; Bono, P.; Hellman, J.; Leu, T.; Jalkanen, S. Cloning of vascular adhesion protein 1 reveals a novel multifunctional adhesion molecule. *J. Exp. Med.* **1998**, *188*, 17–27.

(47) Holt, A.; Smith, D. J.; Cendron, L.; Zanotti, G.; Rigo, A.; Di Paolo, M. L. Multiple binding sites for substrates and modulators of semicarbazide-sensitive amine oxidases: kinetic consequences. *Mol. Pharmacol.* **2008**, *73*, 525–538.

(48) Berman, H. M.; Westbrook, J.; Feng, Z.; Gilliland, G.; Bhat, T. N.; Weissig, H.; Shindyalov, I. N.; Bourne, P. E. The Protein Data Bank. *Nucleic Acids Res.* **2000**, *28*, 235–242.

(49) Lovell, S. C.; Word, J. M.; Richardson, J. S.; Richardson, D. C. The penultimate rotamer library. *Proteins* **2000**, *40*, 389–408.

(50) Lehtonen, J. V.; Still, D. J.; Rantanen, V. V.; Ekholm, J.; Björklund, D.; Iftikhar, Z.; Huhtala, M.; Repo, S.; Jussila, A.; Jaakkola, J.; Pentikäinen, O.; Nyrönen, T.; Salminen, T.; Gyllenberg, M.; Johnson, M. S. BODIL: a molecular modeling environment for structure−function analysis and drug design. *J. Comput.-Aided Mol. Des.* **2004**, *18*, 401–419.

(51) *SYBYL*, version 7.3; Tripos International (1699 South Hanley Rd, St. Louis, MO, 63144, U.S.).

(52) De Colibus, L.; Li, M.; Binda, C.; Lustig, A.; Edmondson, D. E.; Mattevi, A. Three-dimensional structure of human monoamine oxidase A (MAO A): relation to the structures of rat MAO A and human MAO B. *Proc. Natl. Acad. Sci. U.S.A.* **2005**, *102*, 12684–12689.

(53) Frisch, M. J.; Trucks, G. W.; Schlegel, H. B.; Scuseria, G. E.; Robb, M. A.; Cheeseman, J. R.; Montgomery, J. A., Jr.; Vreven, T.; Kudin, K. N.; Burant, J. C.; Millam, J. M.; Iyengar, S. S.; Tomasi, J.; Barone, V.; Mennucci, B.; Cossi, M.; Scalmani, G.; Rega, N.; Petersson, G. A.; Nakatsuji, H.; Hada, M.; Ehara, M.; Toyota, K.; Fukuda, R.; Hasegawa, J.; Ishida, M.; Nakajima, T.; Honda, Y.; Kitao, O.; Nakai, H.; Klene, M.; Li, X.; Knox, J. E.; Hratchian, H. P.; Cross, J. B.; Adamo, C.; Jaramillo, J.; Gomperts, R.; Stratmann, R. E.; Yazyev, O.; Austin, A. J.; Cammi, R.; Pomelli, C.; Ochterski, J. W.; Ayala, P. Y.; Morokuma, K.; Voth, G. A.; Salvador, P.; Dannenberg, J. J.; Zakrzewski, V. G.; Dapprich, S.; Daniels, A. D.; Strain, M. C.; Farkas, O.; Malick, D. K.; Rabuck, A. D.; Raghavachari, K.; Foresman, J. B.; Ortiz, J. V.; Cui, Q.; Baboul, A. G.; Clifford, S.; Cioslowski, J.; Stefanov, B. B.; Liu, G.; Liashenko, A.; Piskorz, P.; Komaromi, I.; Martin, R. L.; Fox, D. J.; Keith, T.; Al-Laham, M. A.; Peng, C. Y.; Nanayakkara, A.; Challacombe, M.; Gill, P. M. W.; Johnson, B.; Chen, W.; Wong, M. W.; Gonzalez, C.; Pople, J. A. *Gaussian 03*; Gaussian, Inc.: Pittsburgh, PA, 2003.

(54) Bayly, C. I.; Cieplak, P.; Cornell, W. D.; Kollman, P. A. A Well-behaved electrostatic potential based method using charge restraints for deriving atomic charges: the RESP model. *J. Phys. Chem.* **1993**, *97*, 10269.

(55) Wang, J.; Wang, W.; Kollman, P. A.; Case, D. A. Automatic atom type and bond type perception in molecular mechanical calculations. *J. Mol. Graphics Modell.* **2006**, *25*, 247–260.

(56) Phillips, J. C.; Braun, R.; Wang, W.; Gumbart, J.; Tajkhorshid, E.; Villa, E.; Chipot, C.; Skeel, R. D.; Kale, L.; Schulten, K. Scalable molecular dynamics with NAMD. *J. Comput. Chem.* **2005**, *26*, 1781–1802.

(57) Duan, Y.; Wu, C.; Chowdhury, S.; Lee, M. C.; Xiong, G.; Zhang, W.; Yang, R.; Cieplak, P.; Luo, R.; Lee, T.; Caldwell, J.; Wang, J.; Kollman, P. A point-charge force field for molecular mechanics simulations of proteins based on condensed-phase quantum mechanical calculations. *J. Comput. Chem.* **2003**, *24*, 1999–2012.

(58) Wang, J.; Wolf, R. M.; Caldwell, J. W.; Kollman, P. A.; Case, D. A. Development and testing of a general amber force field. *J. Comput. Chem.* **2004**, *25*, 1157–1174.

(59) Feller, S. E.; Zhang, Y.; Pastor, R. W.; Brooks, B. R. Constant pressure molecular dynamics simulation: the Langevin piston method. *J. Chem. Phys.* **1995**, *103*, 4613.

(60) Schlick, T.; Skeel, R. D.; Brunger, A. T.; Kalé, L. V.; Board, J. A. J.; Hermans, J.; Schulten, K. Algorithmic challenges in computational molecular biophysics. *J. Comput. Phys* **1999**, *151*, 9–48.

(61) Darden, T.; York, D.; Pedersen, L. Particle mesh Ewald: an W log(N) method for Ewald sums in large systems. *J. Chem. Phys.* **1993**, *98*, 10089–10092.

(62) Ryckaert, J.; Ciccotti, G.; Berendsen, H. J. Numerical integration of the Cartesian equations of motion of a system with constraints: molecular dynamics of *n*-alkanes. *J. Coput. Phys* **1977**, *23*, 327.

(63) Salter-Cid, L. M.; Wang, E. Y.; MacDonald, M. T.; Zhao, J. PCT Int. Appl. WO 2005082343, 2005.